Supporting Information

Supplement to: Filament nucleation tunes mechanical memory in active polymer networks

Vikrant Yadav, Deb S. Banerjee, A. Pasha Tabatabai, David R. Kovar, Taeyoon Kim, Shiladitya Banerjee, and Michael P. Murrell*

Supplemental Methods

Particle Tracking. Individual myosin thick filaments are monitored by spot tracking of the center of fluorescence intensity in Imaris (Bitplane). The positions over time are recorded for calculation of the Mean Square Displacement (MSD).

Mean-Squared Displacement (MSD). The positions of myosin thick filaments ($\vec{r_i}$) are identified by the centroid of their fluorescence intensity and their trajectories are assembled by a minimization of least square method (Imaris, Bitplane). The MSD will take the form:

$$MSD(\Delta t) = \langle \frac{1}{N} \sum_{i=1}^{N} \left(\vec{r_i}(t) - \vec{r_i}(t + \Delta t)\right)^2 \rangle \sim \Delta t^{\alpha} \quad (1)$$

where α is a power law scaling factor. For $\alpha<1$, the network behaves subdiffusively, illustrative of caging or elastic-like behavior. For $\alpha=1$, the network behaves as a fluid as the probes move diffusively. For $\alpha>1$, there probes behave super-diffusively, being driven by active forces. N is the total number of myosin thick filaments.

Mesh Size Calculation: To estimate the size distribution of mesh made by filaments we extract a 500x10 pixel long element from the experimental images. The extracted element is average along its short axis giving a 500x1 pixel long intensity profile. We normalize the intensities by the mean intensity of element. We then choose a cutoff to segment the intensity profile into region with filaments and region with no filaments and record the length of each filament free region. The process is repeated at multiple locations in the image and in various images. Finally we average over all measurements to get the mean mesh size.

Filament Bending Energy. Bent filaments are interpreted as beams with a bending energy

$$E_{bend} = \frac{LEI}{2R_c^2} \quad (2)$$

where *EI* is the flexural rigidity of actin, L is the contour length of the polymer, and R_c is the radius of curvature of the bend. We manually fit circles to filament bends in ImageJ, which generates a bias towards higher curvatures.[1] At low formin concentrations, filaments are long and contain multiple bends. At medium formin concentrations, it is difficult to discern one filament from bundles of filaments. Consequently, we define $L = R_c$. We define $E = 2 \times 10^9$ N/m^2 and the cross-sectional radius of an actin filament to be 4 nm.

Estimation of Frank Free Energy. If $\hat{n}$ is the director field of the actin network then the Frank free energy of the network is given by

$$E = \frac{1}{2}K_{11}(\nabla \cdot \hat{n})^2 + \frac{1}{2}K_{22}(\hat{n} \cdot \nabla \times \hat{n})^2 + \frac{1}{2}K_{33}(\hat{n} \times \nabla \times \hat{n})^2 \quad (3)$$

Where $|\hat{n}| = 1$, and first, second, and third term in the equation correspond to splay, twist, and bend in the director field respectively. As the system is quasi 2D at 100 nM formin, we can neglect K_{22}. Then using the approximation $K_{11} = K_{33} = K$, we have

$$\frac{E}{K} = \frac{1}{2}(\nabla \cdot \hat{n})^2 + \frac{1}{2}(\hat{n} \times \nabla \times \hat{n})^2 \quad (4)$$

Director field calculations. The director field is calculated using custom Matlab code as described previously.[2] Briefly, a director field, $\hat{n}$ is created from images of fluorescently labeled F-actin and the images are divided into small, overlapping 3.5 μm by 3.5 μm windows, and the local orientation director is calculated for each window.[3] Each window is then Gaussian filtered and transformed into Fourier space using a 2D fast Fourier Transform (FFT). Then, the axis of

the least second moment is calculated from the second order central moments of the transformed window. The angle of the local F-actin director is defined as orthogonal to this axis.

Fluorescence Recovery After Photobleaching (FRAP). For fluorescence images of both F-actin and FITC-DHPE, a circular region is drawn in the image over which the fluorescence, I is measured. Simultaneously, in a region far from the photo-bleached region, the fluorescence I_{bg} is measured. Then, the quotient, I/I_{bg} is taken over time. This value is fit to the following equation:

$$I/I_{bg} = b_1 - b_2 * e^{-t/\tau_1}. \quad (5)$$

There are three coefficients fit, b_1, b_2 and τ_1 which is the exponential timescale for the recovery of fluorescence and the principal indicator of turnover.

Image Autocorrelations. For fluorescence images of F-actin at steady-state, we characterize the effective network viscoelasticity through autocorrelations. Images are background subtracted using a rolling ball region of 50 pixel, and Gaussian filtered with a filter of standard deviation 2 in ImageJ before analysis. Autocorrelations are calculated as

$$\langle I(t)I(t+\Delta t)\rangle \sim e^{-\Delta t/\tau_2} \quad (6)$$

for time differences of Δt in image intensities I. An exponential fit gives timescale τ_2 which is the exponential timescale for the decay in actin intensity over time and an indicator for network viscoelasticity.

Myosin Motion to Probe Network Mechanics. To further understand network mechanical properties beyond what is driven thermally, we embed probes in networks of high formin concentration to measure F-actin network fluctuations. However, as an alternative to embedding

passive particles as is commonly done in microrheology , instead we use active probes [4-6]. The F-actin gels are thin and may resist the entanglement of probe particles, therefore we add myosin thick filaments which are well suited for their capacity to adhere and embed within the network. In myosin experiments, Alexa-642 labelled smooth muscle myosin dimers are added at 50 nM to the sample to polymerize. Prior to addition, the smooth muscle myosin is spun with 15 μM F-actin stabilized with 30 μ dark phalloidin in F-buffer supplemented to 0.45M KCl at 39,000 rpm at 4C for 30 min. The supernatant is removed, leaving behind enzymatically inactive motor in the pellet, thus reducing the propensity for excess 'crosslinking' in our assay.

After approximately 20 minutes, dimers of smooth muscle myosin II are added slowly to the F-actin gel, and thick filaments polymerize into large (~1 μm) assemblies over time. We add myosin filaments at densities that are too low to induce net contractility, as has been shown to occur at a critical threshold.[7, 8] As thick filaments polymerize (~20 min), they embed into the F-actin network (SFig 2AB). Myosin motors will move, in part due to thermal fluctuation and in part due to its active motility. We quantify these effects using the Mean-Square Displacement (MSD) of their motion within the network (SFig 2C). Consistent with previous studies, we find that at short times, myosin motion is sub-diffusive, although transitions to a diffusive regime at between 2-10 minutes.[9] Relatedly, we measure the Non-Gaussian Parameter (NGP) which indicates the extent to which displacements are both larger and smaller than what is expected by a Gaussian distribution of displacements (SFig 2D,E). The short-time behavior is non-Gaussian, with both exponential tails indicative of large displacements, as well as a peak in small, near zero displacements. The large displacements are persistent walks by myosin, while the small displacements indicate an inhibition to motion. The latter dominates, leading to sub-diffusive behavior. At longer times, myosin motion is Gaussian, accounting for the diffusivity. These

behaviors are consistent with early time 'caging' and elasticity, and longer time 'escape' and viscous behavior, as has been seen in gels of colloidal particles.[10] Analysis of the NGP (SFig 2E) also shows a characteristic time of between 2 and 10 minutes. This suggests an elasticity below 2 minutes, viscosity beyond 10 minutes, and a viscoelastic response in between. The timescale is comparable for τ_1, (~ 10 min) for the turnover time for gel nucleated by 1 μM mdia1.

Simulation of Growth of Actin Filaments. We simulate our experiments using a simple stochastic model. The simulations are initialized with total number of g-actin monomers in simulation that we call pool size N_p, and number of formin nucleators N_f. A monomer in the simulation is a coarse grained approximation. We ignore any detailed interaction between formin and filament. The role of formin is limited to creating filaments of a specific length from the monomer pool. At each time step we estimate the number fraction of free g-actin in the simulation (m). If there is sufficient free g-actin, formins will add new N_f actin filaments of length L_0m monomers. We then re-estimate the amount of free g-actin and scale it with number of filaments in the system. This ratio gives us an estimate of free g-actin available per f-actin filament to polymerize. We then generate a random number and compare it with this ratio. When the random number is smaller than this ratio, we increment the length of the filament by 1 monomer, otherwise we reduce the length by 1. This simple mechanism ensures that polymerization of actin filaments dominates at earlier stages, but as the pool of free g-actin depletes, depolymerization sets in. At equilibrium, the amount of material available for new filaments, as well as for growth of old filaments is equal to the amount of material released by depolymerization of filaments in previous steps. At each time step we record, number of actin filaments and mean length of filaments. This simulation runs for 10^4 steps, and we average over 20 runs for the results shown in the paper.

Parameter	Symbol	Value
Number of g-actin monomers/pool size	N_p	$5x10^6$ - $4x10^7$
Number of formin nucleators	N_f	10-1000
Rate of growth of actin from formin	R_f	100 monomer/time step
Rate of growth of free actin	K^+	Variable
Rate of decay of free actin	K^-	Variable
Time step	t_{sim}	10^4
Length of actin filament produced by formin	L_0	100 monomer

Simulation of Growth of Actin Filaments: This is a list of multiple time scales that appear in this paper:

Time scale	Symbol (reference figure)	Value
Formin mediate growth (fast)	- (Fig 1B)	O(seconds)
Profilin mediated growth (slow)	- (Fig 1B)	O(minutes)
Fast network growth	R_1 (Fig 1E)	0-20 minutes

Slow network growth	R_2 (Fig 1E)	>20 minutes
Turnover time scale	τ_1 (Fig 2D)	~10^0-10^1 minutes
Relaxation time scale	τ_2 (Fig 4D)	~10^1-10^3 minutes

Mechanics of Curved Filament Growth: To understand the mechanistic origin of curved F-actin assembly at intermediate Formin concentrations, we implemented a mean field model of a growing soft filament embedded in a filamentous meshwork. The system consists of n_F semiflexible polymers contained in a volume V at temperature T. The mean filament length at time t is given by L(t), in monomer length units. The filaments are assembled from a finite pool of monomers, of total number N. The filament concentration is given by $c = n_F/V$. The free energy of the system, F, can be written as a sum of chemical potential for filament assembly and mechanical energies associated with filament bending and network deformation,

$$F = E_{growth} + E_{bend} + E_{strain} + E_P \quad (7)$$

where E_{growth} is the chemical energy associated with filament assembly and disassembly, E_{bend} is the potential energy for filament bending, E_{strain} is the local strain energy of the polymer network sensed by a filament, and E_P is the growth pressure from the surrounding network. For simplicity, we neglect entropic contributions. If μ is the chemical potential associated with filament growth, and μ_d is the chemical potential for filament disassembly, then the energy released by filament growth is given by:

$$E_{growth} = -\mu L\left(N - \frac{n_F}{2}\right) + \mu_d L = -\mu L\left(N - \frac{n_F L}{2} - k_d\right) \quad (8)$$

where $k_d = \mu d/\mu$. The potential energy for filament bending and network strain energy are given by:

$$E_{bend} = \frac{L_p}{2}\frac{L}{R^2} \quad (9)$$

$$E_{strain} = \frac{G(c)V}{2}\varepsilon^2 \quad (10)$$

where R is the radius of curvature of the filament, L_p is the persistence length, G(c) is the elastic modulus and ε is the strain in the filamentous network. In the mean field approximation, we assume that the local strain in the network arises from filament bending such that $\varepsilon = 1 - d/L$, where $d = 2R\sin(\theta/2)$ is the filament end-to-end distance, with $\theta = L/R$. Growth of the surrounding filamentous network will impart a mechanical pressure, P, on the filaments, giving rise to the energy

$$E_P = -P(c)A\left(L - 2R\sin\left(\frac{\theta}{2}\right)\right) \quad (11)$$

where A is the area of cross-section of a filament. The effective free energy is then given by

$$F(R,L) = -\mu L\left(N - cV\frac{L}{2} - k_d\right) + \frac{L}{2}\frac{L_p}{R^2} + \frac{G(c)V}{2}\left(1 - \frac{2R}{L}\sin\left(\frac{\theta}{2}\right)\right)^2 - P(c)(L - 2R\sin(\theta/2)) \quad (12)$$

where $c = n_F/V$. We assume that the elastic modulus of the F-actin network is dependent on F-actin concentration as $G(c)V \sim g_0c^2$, and the growth pressure is assumed to be linearly proportional to filament concentration $P(c)A \sim p_0c$, where g_0 and p_0 are constants.[11] We apply the above effective theory to describe curved F-actin assembly at intermediate concentrations. For simplicity we assume that an average filament is uniformly curved with a radius of curvature $R = L/\theta$. For computational convenience, we rewrite the free energy as a function of L and θ

$$F(L,\theta) = -\mu L\left(N - cV\frac{L}{2} - k_d\right) + \frac{L_p\theta^2}{2L} + g_0c^2\left(1 - \chi\left(\frac{\theta}{2}\right)\right)^2 - p_0cL(1 - \chi(\theta/2)) \qquad (13)$$

where $\chi(\theta) = \sin(\theta)/\theta$. The dynamics of length L and the angle θ are then given by:

$$\dot{L} = -\eta_L\frac{\partial F}{\partial L}$$

$$= \eta_L\left(\mu(N - cVL - k_d) + \frac{L_p\theta^2}{2L} + p_0c\left(1 - \chi\left(\frac{\theta}{2}\right)\right)\right) \qquad (14)$$

and

$$\dot{\theta} = -\eta_\theta\frac{\partial F}{\partial \theta}$$

$$= -\eta_\theta\left(\frac{L_p\theta}{L} - g_0c^2\left(1 - \chi\left(\frac{\theta}{2}\right)\right)^2\chi'\left(\frac{\theta}{2}\right) - \frac{1}{2}p_0c\chi'\left(\frac{\theta}{2}\right)\right) \qquad (15)$$

where η_L and η_θ are mobility constants and $\chi`(\theta) = \partial\chi(\theta)/\partial\theta$. We solve the above equations to obtain the dynamics of L(t) and θ(t), for a given filament concentration, c. From these data, we can compute the dynamics of filament curvature using the relation $R^{-1}(t) = \theta(t)/L(t)$. The results

of numerical solution to the differential equations are shown in Fig. 3J in main text, for n_F/N = 0.12. For this intermediate value of n_F/N, the growing filament quickly attains a curved morphology via buckling due to mechanical pressure from the surrounding network. The filament then continues to elongate at a constant curvature. This hoop-like growth of the filament acts as a template for curved self-assembly of other polymers in its vicinity. We further investigate the dependence of steady-state filament curvature on filament concentration. Figure 3I in main text shows that R^{-1} exhibits a non-monotonic dependence of n_F/N, the ratio of Formin to G-actin concentrations. At low n_F/N, the filamentous network is dilute and does not generate sufficient force on a growing filament, which assembles in an approximate straight morphology. At intermediate values of n_F/N, the competition between growth and bending leads to maximum curvature of growing filaments. At higher values of n_F/N, filament lengths are smaller than L_p and are unable to bend. This results in a dense meshwork of short rod-like filaments.

Supplemental Figures

Phenotype	1 nM	10 nM	100 nM	1 μM
Total N	2	13	11	29
Loose/Entangled Filaments	2	12	3	2
Swirls/Vortices	0	0	8	3
Vertical/Dense	0	0	0	21
Failed Polymerization	0	1	1	3
%	100	92	72.7	72

Supplementary Figure 1. Statistics of Qualitatively Distinct Phenotypes. There are three principal phenotypes: loose, entangled filaments that occurs at and below 10 nM formin, swirls/vortices principally at 100 nM, and a vertical/dense network at 1 μM. Total experimental samples is N=55. 28 Control Samples were included, which include no profilin, no mdia1, no NTA, and different independent experiments for these controls. Thus, the total sample size is N=83 independent experiments.

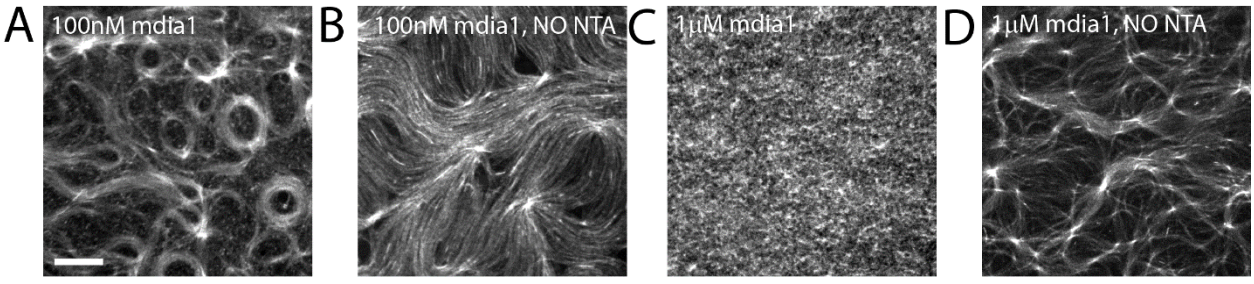

Supplementary Figure 2. F-actin coupling to bilayer influences network structure. A comparison of steady-state F-actin network structures for 100 nM mdia1 with nickel lipid (A) and without nickel lipid (B). Without nickel lipid, actin filaments are formed in solution, instead of at the membrane surface and are then crowded down to the surface through depletion forces (via Methylcelluose). These filaments organize into nematic like structures, consistent with previous work [8, 12]. Steady-state F-actin structures for 1 μm mdia1 with nickel lipid (C) and without nickel lipid (D). Scale bar is 10 μm.

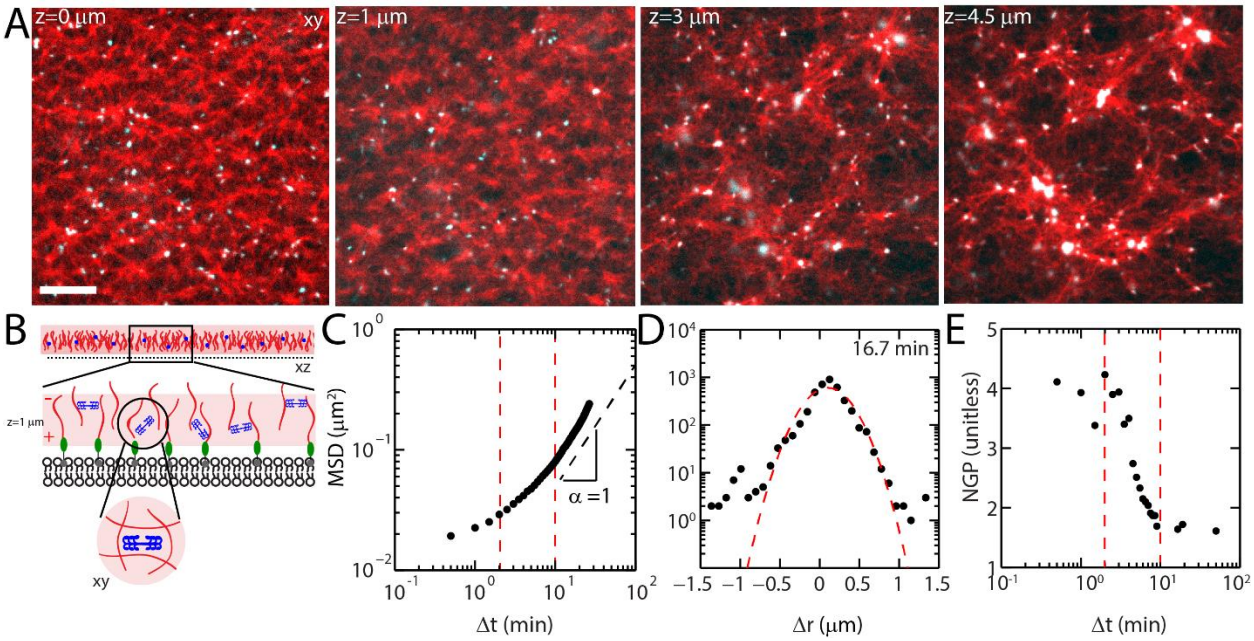

Supplementary Figure 3. Depth dependent structure of network after contraction by myosin. (A) After the addition of myosin (cyan), the F-actin network structure (A) depends on depth. The F-actin network is contracted into heterogeneous puncta of high concentration actin at z=4.5 μm, while it remains unchanged at the base of the gel (z=0 μm). This suggests that the bottom of the network is adherent to the bilayer. As formin processively elongates filaments with a finite probability of detaching at each step, the probability of release may be proportional to the length of the filament. As the length of the filament is shortest at 1 mM actin, the adhesion may be greater. The lipid bilayer is located at z=0 μm. Scale bar is 10 μm. (B) Thick filaments of smooth muscle myosin II embed within the F-actin network. (C) The motion of the myosin molecules is calculated by the Mean-Square Displacement (MSD) which shows subdiffusive displacement at short times, and diffusive motion at long times. (D) The Van Hove correlation is a distribution of filament displacements at a set time, which shows exponential tails indicating large steps and a larger than expected number of short steps. (E) The Non-Gaussian Parameter (NGP) indicates two timescales of myosin motion within the F-actin network, the latter being 10

minutes until the network behaves more diffusively – precisely the turnover time as measured for 1 μM formin networks.

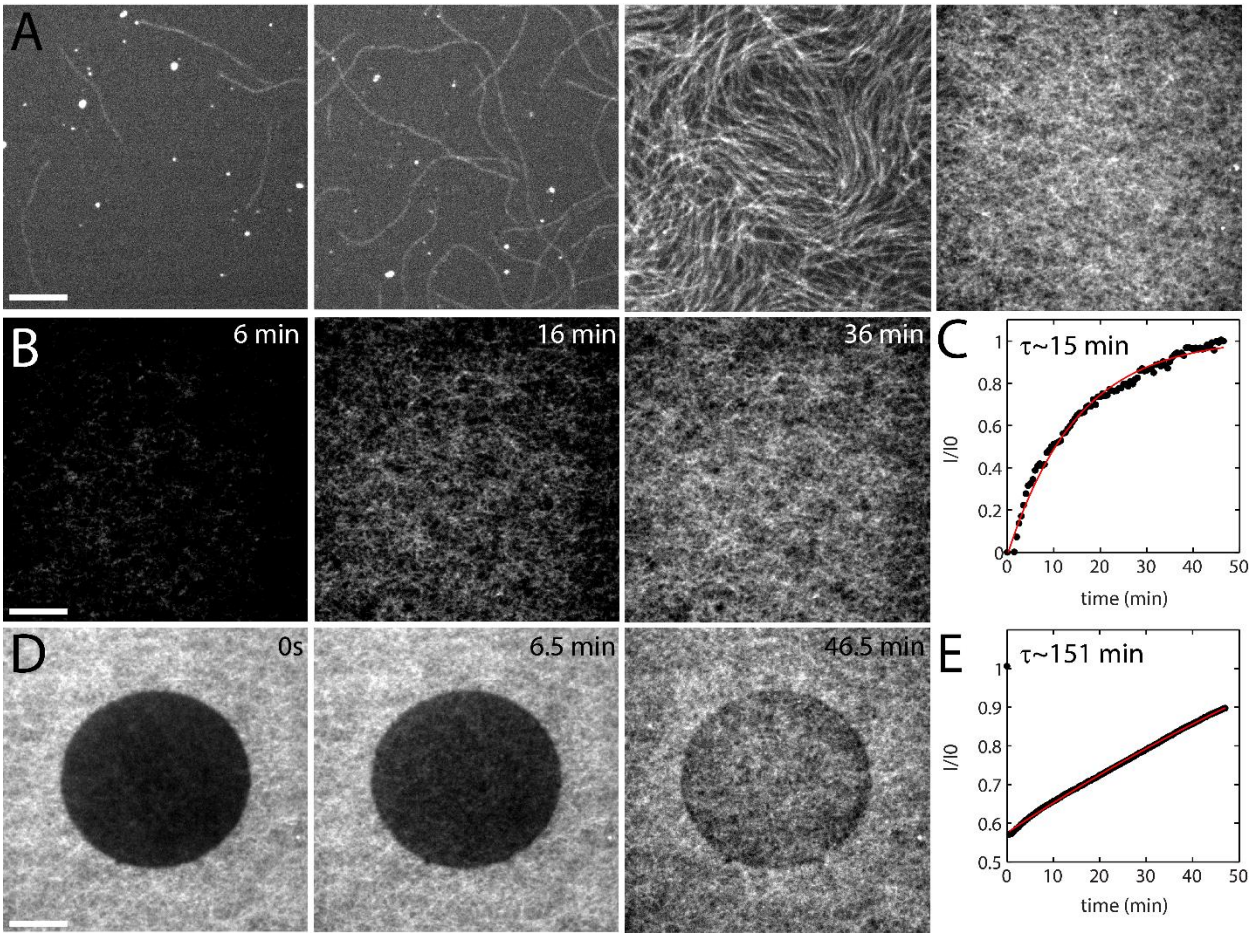

Supplementary Figure 4. F-actin recovery in the absence of nucleator. (A) Each panel is a different region within the same sample. F-actin within a single sample is very variable in its density when not nucleated from the surface. (B) F-actin growth during polymerization of F-actin in the absence of formin, mdia, or NTA-Ni. (C) Quantification of fluorescence intensity over time. Red line indicates an exponential fit, with a timescale of 15 minutes. (D) Fluorescence recovery after photobleaching of F-actin where turnover is not formin-assisted. (E) Quantification of fluorescence intensity over time. Red line indicates an exponential fit, with a long recovery timescale.

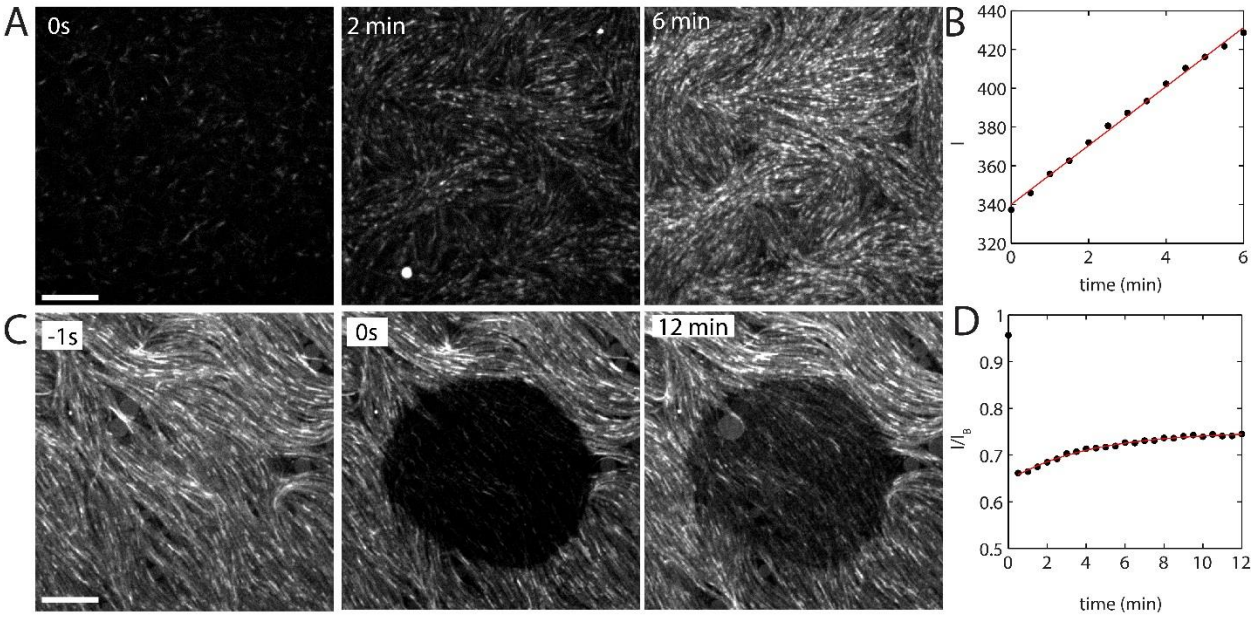

Supplementary Figure 5. Phalloidin-labelled F-actin does not recover. (A) F-actin fluorescence over time for Alexa-568 labelled F-actin is stabilized by phalloidin. (B) Quantification of F-actin fluorescence over time.

Movie Captions

Movie 1. F-actin network growth with low concentration formin. Growth of F-actin network with 10 nM mdia1. Time is hours:minutes:seconds. Scale bar is 10 μm.

Movie 2. F-actin network growth with medium concentration formin. Growth of F-actin network with 100 nM mdia1. Time is minutes:seconds. Scale bar is 10 μm.

Movie 3. F-actin network growth with high concentration formin. Growth of F-actin network with 1 μM mdia1. Time is minutes:seconds. Scale bar is 10 μm.

Movie 4. Thermal fluctuations of F-actin network. Thermal fluctuations of F-actin network z=0 μm and z=1 μm with 1 μM mdia1. Time is minutes:seconds. Scale bar is 10 μm.

Movie 5. Fluorescence recovery after photobleaching of F-actin network. F-actin network is photobleached in a circular region. Active polymerization of new F-actin results in the fluorescence recovery in photobleached region. Note: F-actin structure before and after photobleaching is the same. Time is minutes:seconds. Scale bar is 10 μm.

Movie 6. Two-color fluorescence recovery after photobleaching of F-actin network. An actin network is first polymerized with 568 nm fluorescent actin, then 642 nm fluorescent actin is added. The actin network is photobleached in a circular region for both 568 nm (left) and 642 nm (right). Fluorescence recovery is faster for 642 nm actin. Both actin channels recover structures with the geometries as the pre-photobleached geometries. Time is minutes:seconds. Scale bar is 10 μm.

References

1. Schindelin J, A.-C.I., Frise E, Kaynig V, Longair M, Pietzsch T, Preibisch S, Rueden C, Saalfeld S, Schmid B, Tinevez JY, White DJ, Hartenstein V, Eliceiri K, Tomancak P, Cardona A, *Fiji: an open-source platform for biological-image analysis.* Nature Methods, 2012. **9**: p. 7.
2. Seara, D.S., et al., *Entropy production rate is maximized in non-contractile actomyosin.* Nat Commun, 2018. **9**(1): p. 4948.
3. Cetera, M., et al., *Epithelial rotation promotes the global alignment of contractile actin bundles during Drosophila egg chamber elongation.* Nat Commun, 2014. **5**: p. 5511.
4. Lau, A.W., et al., *Microrheology, stress fluctuations, and active behavior of living cells.* Phys Rev Lett, 2003. **91**(19): p. 198101.
5. Crocker, J.C., et al., *Two-point microrheology of inhomogeneous soft materials.* Phys Rev Lett, 2000. **85**(4): p. 888-91.
6. Gardel, M.L., et al., *Microrheology of entangled F-actin solutions.* Phys Rev Lett, 2003. **91**(15): p. 158302.
7. Linsmeier, I., et al., *Disordered actomyosin networks are sufficient to produce cooperative and telescopic contractility.* Nature Communications, 2016. **7**: p. 12615.
8. Murrell, M. and M.L. Gardel, *Actomyosin Sliding is Attenuated in Contractile Biomimetic Cortices.* Mol Biol Cell, 2014.
9. Amblard, F., et al., *Subdiffusion and Anomalous Local Viscoelasticity in Actin Networks.* Phys Rev Lett, 1996. **77**(21): p. 4470-4473.
10. Weeks, E.R. and D.A. Weitz, *Subdiffusion and the cage effect studied near the colloidal glass transition.* Chemical Physics, 2002. **284**(1-2): p. 361-367.
11. Gardel, M.L., et al., *Elastic behavior of cross-linked and bundled actin networks.* Science, 2004. **304**(5675): p. 1301-5.
12. Murrell, M.P. and M.L. Gardel, *F-actin buckling coordinates contractility and severing in a biomimetic actomyosin cortex.* Proc Natl Acad Sci U S A, 2012. **109**(51): p. 20820-5.